Theoretical and Applied Fracture Mechanics 109 (2020) 102759

Contents lists available at ScienceDirect

Theoretical and Applied Fracture Mechanics

journal homepage: www.elsevier.com/locate/tafmec

Crack growth prediction for irradiated stainless steels under the combined fatigue-creep loading

Robert W. Fuller[a], Jutima Simsiriwong[b,c,*], Nima Shamsaei[c,d]

[a] Entergy Operations, Grand Gulf Nuclear Station, Port Gibson, MS 39150, USA
[b] School of Engineering, University of Florida, Jacksonville, FL 32224, USA
[c] National Center for Additive Manufacturing Excellence (NCAME), Auburn University, Auburn, AL 36849, USA
[d] Department of Mechanical Engineering, Auburn University, Auburn, AL 36849, USA

ARTICLE INFO

Keywords:
Strip-yield model
Neutron irradiation
Creep-fatigue
Elevated temperature
Crack growth estimation

ABSTRACT

A methodology is presented in this study for estimating the crack growth of austenitic stainless steel Types 304, 304L, 316, and 316L, which are commonly used as structural materials in nuclear pressure vessels. These structural components are typically subjected to neutron irradiation and combined loadings, including repeated mechanical stresses (i.e., fatigue) resulting from startups and shutdowns, as well as creep due to on-load periods at elevated temperature. In this study, the fatigue crack length was estimated using a strip-yield based fatigue crack growth model. The model is extended to include the effects of creep deformation in a presence of hold-times, and expanded to include the effects of irradiation. Reasonable crack growth estimations are obtained for selected materials under various combined loading conditions when compared to the experimental data available in the literature.

1. Introduction

Reactor internals are typically susceptible to aging-related degradation due to their operating conditions (i.e., applied thermal and mechanical loading, fast neutron flux exposure, reactor coolant water environment, etc.). In most cases, it is recognized that mechanical failure in many of these structural components has been attributed to fatigue. An example includes the jet pump beam assembly failure of a boiling water reactor (BWR) at the Grand Gulf Nuclear Station in 1993 [1]. Inspection of the failed jet pump beam revealed a crack of more than three-quarters of the cross section of the intact end. The probable cause of failure was concluded to be the intergranular stress corrosion crack that covered 80% of the fracture surface, while the remaining surface was fatigue striations that may have resulted in a loss of preload [1]. Other examples related to fatigue failure of structural components in nuclear power plants have been reported in nozzles, pumps, and piping systems [2,3].

Generally, the effects of fatigue damage on material deterioration can be further exacerbated by the presence of thermal loading, hold-time, and high-temperature water coolant environments [4]. Although the American Society of Mechanical Engineers (ASME) Boiler and Pressure Vessel Code specifies fatigue design curves for the construction of nuclear power plant components [5], the effects of hold-time during the loading cycle and dissolved oxygen (DO) environment on the fatigue resistance of a material are not specifically addressed. The problem is compounded by the fact that the available fatigue data for irradiated materials with environment effects is limited. Such experiment is typically expensive from a time and cost perspective.

In terms of the mechanical behavior of irradiated materials, the effects of neutron irradiation on tensile properties have been established to some extent, predominantly for austenitic stainless steels (SS) that are widely used as structural materials for internal reactor components [6]. On the other hand, relatively few data on fatigue crack growth rate for irradiated materials are available, and the majority are those subjected to irradiation in fast breeder reactors. For 20% cold-worked and annealed Type 316 SS, Michel and Smith [7] observed minimum effects of irradiation of 11 displacements per atom (dpa) in the Experimental Breeder Reactor II (EBR-II) on fatigue crack growth rate, at test temperature of 427 °C in air. When increased test temperature to 593 °C, it was reported that the crack growth rate increased by a factor of 10 for cold-worked Type 316 SS, relative to un-irradiated material [7].

Abbreviations: ASME, American Society of Mechanical Engineers; BWR, boiling water reactor; CT, compact-tension; DC, direct-current; DO, dissolved oxygen; dpa, displacements per atom; ppb, parts per billions; ppm, parts per millions; PWR, pressurized water reactor; SS, stainless steel

* Corresponding author at: School of Engineering, University of Florida, Jacksonville, FL 32224, USA.
E-mail address: j.simsiriwong@unf.edu (J. Simsiriwong).

https://doi.org/10.1016/j.tafmec.2020.102759
Received 8 June 2020; Received in revised form 31 July 2020; Accepted 1 September 2020
Available online 04 September 2020
0167-8442/

Nomenclature

A_s	secondary creep strain coefficient
a	crack length, m
a_i	initial crack length, m
B_n	functions of flow stress
C	coefficient in the modified Paris-Elber equation
C^*	C contour integration
C_1, C_2, C_3, C_4, C_5	constants in the Newman relationship
$(C_t)_{avg}$	small scale creep parameter
$dose$	dose in dpa
d_o	dose constant, dpa
$\frac{da}{dN}$	change in crack length in one cycle, m/cycle
$\left(\frac{da}{dN}\right)_{fatigue}$	change in crack length due to fatigue in one cycle, m/cycle
$\left(\frac{da}{dt}\right)_{creep}$	crack extension rate due to creep for a given time differential, m/sec
dt	change in time, sec
E	modulus of elasticity, MPa
$f(x_i)$	displacement of crack for an applied stress, S_{max}
G	shear modulus, MPa
$g(a,x_j)$	displacement for the contact stresses applied in the plastic zone
$h(x)$	weight function
$I_{N'}$	non-dimensional function of the plastic strain hardening exponent
J	hardening exponent in the Andrade's Law equation
k	coefficient of resistance in the Andrade's Law equation
K_C	fracture toughness, MPa-m^{½}
K_{max}	maximum applied stress intensity factor, MPa-m^{½}
K_{min}	minimum applied stress intensity factor, MPa-m^{½}
K_o	opening stress intensity factor, MPa-m^{½}
K_{th}	threshold stress intensity factor, MPa-m^{½}
M	viscosity exponent in the Andrade's Law equation
m	exponent in the modified Paris-Elber equation
N'	plastic strain hardening exponent
N	number of cycles
n'	secondary creep exponent for Types 304 and 304L SS
n^*	secondary creep exponent for Types 316 and 316L SS
Q	activation energy, J/mole
R	load ratio
R^*	Boltzman gas constant, J/(mole-°K)
r_c	radius of creep process zone, m
S	applied remote uniform stress over the crack surface, MPa
S_{max}	maximum applied stress, MPa
S_0	crack opening stress, MPa
T	temperature, °K
t	time, sec
t_{hold}	hold-time, sec
t_i	incubation time, sec
U	crack closure parameter
W	specimen width, m
β	Irwin's crack length correction factor
Δa	change in crack length for a given cycle, m
ΔK	stress intensity factor range, MPa-m^{½}
ΔK_{eff}	effective stress intensity factor range, MPa-m^{½}
ΔK_0	effective threshold stress intensity factor range, MPa-m^{½}
ΔK_{th}	threshold stress intensity factor range, MPa-m^{½}
ΔN	change in cycles
α	constraint factor, $\alpha = 1$ for plane stress and $\alpha = 3$ for plane strain
ε_f	creep ductility
ε_o	Primary Creep Strain
ε_p	plastic creep strain
$\dot{\varepsilon}_p$	plastic creep strain rate, 1/sec
ε_s	secondary creep strain
ζ	secondary creep strain coefficient
θ	integration variable for crack incubation
ρ	plastic zone length at the crack tip, m
ρ_{max}	plastic zone size under the maximum applied load, m
σ	stress, MPa
σ_{max}	maximum stress, MPa
σ_o	effective flow stress, MPa
σ_{oi}	flow stress at the end of incubation period, MPa
σ_{oo}	initial effective flow stress when primary creep is initiated at the beginning of the incubation time at the crack tip, MPa
ν	Poisson ratio
ϕ	crack tip opening displacement, m
ϕ_c	critical crack tip opening displacement, m
ϕ_o	initial crack opening displacement due to primary creep, m

At lower neutron fluences, fatigue crack growth at 427 °C of Types 304 and 316 SS irradiated to 6 dpa was reported to be approximately twice higher than those for un-irradiated materials [8]. In contrast, no significant effect was observed for Type 304 SS and cold-worked Type 316 SS irradiated to 0.65 and 4.5 dpa in EBR-II when tested at 427 °C [9]. In a normal water chemistry BWR environment, the data of wrought SS irradiated to 0.75–4 dpa indicated higher fatigue crack growth rate as compared to those for un-irradiated materials, while fatigue crack growth data for materials irradiated to 0.45 dpa suggested a minimum neutron irradiation influence [10,11].

A few studies have been performed to investigate the reactor coolant environment effects on fatigue crack growth on austenitic SS. Shack and Kassner [8] complied the crack growth rate for wrought and cast austenitic SS in several test environments. These include normal BWR water chemistry, BWR water chemistries with added hydrogen (i.e., hydrogen water chemistry), and pressurized water reactor (PWR) coolant chemistry. The data showed that, at small crack growth rates ($> 10^{-10}$ m/s), the growth rates in the normal BWR water chemistry surpassed the ASME design curve (in air) by a factor of approximately 20–30. However, at high crack growth rates, the comparatively small effect of coolant on fatigue crack growth was observed for both BWR and PWR environment [8]. Chopra and Shack [10] reported crack growth rate data for irradiated SS in BWR coolant with DO concentration ranging from 200 parts per billions (ppb) to 8 parts per millions (ppm). Significantly lower crack growth rates were observed for all tests performed in simulated hydrogen water chemistry, as compared to the original guidelines [12], suggesting a beneficial effect of low DO environment on crack growth of irradiated SS [10].

In addition to the applied cyclic loading and environmental condition, crack growth in a nuclear reactor can be enhanced by introducing a constant load for a period of time (i.e., creep). Creep in austenitic stainless steels is generally considered to be significant at temperatures above 0.3 of the melting temperature (T_m) [13]. T_m of a typical austenitic stainless steel is 1430 °C [14], while the operating temperature in BWR applications is approximately 289 °C, which is below 0.3 T_m. Nonetheless, many studies have reported noticeable creep deformation of stainless steels at temperatures below 0.3 T_m threshold, which is known as the low-temperature creep [15–17]. This time-dependent behavior at low temperature for crystalline materials and its related mechanisms have been reviewed in detail in [18]. Furthermore, in the presence of neutron fluxes, creep deformation can be significant at a much lower temperature as reported in [19,20].

The irradiation can lead to the damage event and the physical changes in materials' microstructure, including swelling, growth, phase

change, and segregation. This, in turn, dictates the mechanical behavior of the irradiated materials [21]. As previously mentioned, there are relatively limited studies in the area of fatigue-creep crack formation of irradiated materials, and considerably much less concerning the models for crack growth under such environment and loading conditions. While recognizing that the crack growth behavior of irradiated materials/components is extremely complex and significantly influenced by the material's microstructure, microchemistry, radiation hardening, etc., the objective of this study is to analyze the combined fatigue-creep crack growth data available in the literature for several irradiated austenitic SS with different heat treatments. The experimental data employed in this work are obtained from the simulated light-water reactor internals studies, where crack growth tests were performed in high-temperature water environment with dissolved oxygen concentrations ranging from 200 ppb to 8 ppm. Of particular interest to the present study is the fatigue crack growth of irradiated austenitic SS under high-temperature water coolant environment with a presence of hold-times (i.e., creep deformation). A superposition methodology is presented herein based on fracture mechanics approaches to estimate fatigue crack growth considering the effects of creep as well as elevated temperature water environment.

2. Experimental data

Fatigue crack growth rates of 12 irradiated wrought austenitic SS from [10] and [11] are employed and analyzed in this study. The materials investigated in [10] included Types 304, 304L, 316, and 316L SS. The chemical composition of these alloys with different heat treatments are given in details in [10]. Miniature ¼-T compact tension (CT) specimens were irradiated in BWR (Halden Boiling Water Reactor, Halden, Norway). The radiation was carried out in a helium environment and fluence levels of 0.3–2 × 10^{21} neutrons per square centimeter (n/cm^2) at 288 °C as summarized in Tables 1-4 for Types 304, 304L, 316, and 316L, respectively. The fluence level, material composition, and water chemistry were considered and tabulated in the Tables 1-4. Post-irradiation crack growth experiments were conducted in an enclosed hot cell facility under test conditions that were designed to simulate a BWR environment with operating temperature of core internal components of 289 °C (550 °F) in either normal or hydrogen water chemistry [10].

The crack growth rate tests were performed in two stages; a load-controlled cyclic loading and a constant loading. The cyclic loading stage was first conducted under load ratio, R, of 0.2–0.3 at a frequency of 1–5 Hz, and a maximum stress intensity factor, K_{max}, of 13–16 MPa-√m until a sharp fatigue crack of approximately 0.3–0.5 mm was generated. The load ratio and the rise-time were subsequently increased and transitioned to the constant load stage to achieve an intergranular stress corrosion crack. The crack extension during the tests was obtained using the reversed direct-current (DC) potential difference method. Further details of the experimental setup and testing can be found in [10]. Only crack growth results for the transgranular fatigue crack under the first stage (i.e., load-controlled cyclic loading) will be analyzed in the current study.

In [11], disk-shaped CT specimens were fabricated from Types 304L and 316 SS. Type 304L SS specimens (see Table 3) were solution-annealed, while Type 316 SS (see Table 4) underwent cold-working prior to being soaked in water environment to stabilize to the test condition. The irradiation of specimens was conducted in BOR-60 reactor (Dimitrovgrad, Russia), a sodium-cooled fast neutron reactor, to various neutron fluence levels of 4.8–7.8 dpa under irradiation temperature of 315–325 °C. The crack growth rate tests in [11] were performed in either simulated BWR with hydrogen water chemistry or PWR environment. The test temperature and pressure were approximately 320 °C and 1800 psig, respectively.

Similar to the applied loading in [10], the load-controlled cyclic loading with ratio, R, of 0.2–0.3 at 1–2 Hz frequency, and K_{max} of 10–16 MPa-√m was first applied to the specimens until a fatigue crack is generated. Then the load ratio and rise-time were gradually increased to constant loading to achieve the constant stress intensity factor for stress corrosion cracking. Fatigue crack propagation in [11] was monitored using the DC potential drop method. Again, only the crack growth rate results under cyclic loading will be utilized in the present work.

3. Fatigue – creep crack growth modeling for stainless steels

Crack growth in components subjected to cyclic loading with sufficiently long hold-times or loading/unloading rates is affected by both fatigue and creep deformations [22]. The fatigue loadings in reactor components are usually generated from the flow-initiated oscillatory hydrodynamic forces, which can be susceptible to creep deformation due to possible hold-times [19]. Generally, crack growth models for fatigue-creep interaction can be separated into two components: crack growth resulted from the continuously cyclic loading, and that which accounts for the hold-time effects. In these models, the linear summation of deformation has been employed to interpolate/extrapolate the time-dependent crack growth effects [23]. For a component with a crack of length a that is subjected to a combination of cyclic and constant loadings over a time interval dt, the change of crack length in one cycle $\frac{da}{dN}$ can be obtained by superimposing the crack length per cycle due to fatigue and creep as [22]:

$$\frac{da}{dN} = \left(\frac{da}{dN}\right)_{fatigue} + \left(\frac{da}{dN}\right)_{creep} = \left(\frac{da}{dN}\right)_{fatigue} + \left(\frac{da}{dt}\right)_{creep} t_{hold} \quad (1)$$

where $\left(\frac{da}{dN}\right)_{fatigue}$ is the change in crack length due to fatigue for one cycle, $\left(\frac{da}{dN}\right)_{creep}$ is the change in crack length due to creep for one cycle, $\left(\frac{da}{dt}\right)_{creep}$ is the crack extension rate due to creep, and t_{hold} is the hold-time for a given cycle.

3.1. Modified strip-yield model for fatigue crack growth

The modified strip-yield model [24] was proposed to approximate fatigue crack growth with pre-existing residual stress. The model is an extension of Newman's-analytical model of plasticity-induced crack closure for a middle-crack tension specimen, and modified to leave plastically deformed material along the crack surfaces as the crack advances [25]. Using the method described in [25], crack-opening stresses under loading with various applied stress levels and stress ratios can be determined as a function of crack length and load history. Subsequently, crack-opening stresses can be used to calculate the effective stress intensity factor range, ΔK_{eff}, [26] and the crack growth per cycle, $\frac{da}{dN}$. The three-dimensional features of cracks were taken into account by introducing a constraint factor related to the tensile yield stress, as discussed in detail in [25].

While the initial modified strip-yield model by Newman [25] was developed for a center-crack in a finite-width plate under uniform

Table 1
Fatigue crack growth specimens and test conditions for Type 304 stainless steels [10].

Test #	Specimen #	Pre-treatment	Radiation Condition	Test Condition
CGRI JR-31	85-3TT	Sensitized 10.5 h at 600 °C	1.44 × 10^{21} n/cm^2 (2.16 dpa) at ≈ 289 °C	High-purity water with 300–350 ppb DO at 289 °C

Table 2
Fatigue crack growth specimens and test conditions for Type 304L stainless steels [10,11].

Reference	Test #	Specimen #	Pre-treatment	Radiation	Test Condition
[10]	CGRI-12	C3-A	Heat C3*	3.0×10^{20} n/cm^2 (0.45 dpa) at ≈ 288 °C	Water with ≈300 ppb DO at 289 °C
	CGRI-07	C3-B	Heat C3*	9.0×10^{20} n/cm^2 (1.35 dpa) at ≈ 288 °C	Water with 250–300 ppb DO at 289 °C
	CGRI-08	C3-C	Heat C3*	2.0×10^{21} n/cm^2 (3.0 dpa) at ≈ 288 °C	Water with ≈ 300 ppb DO at 289 °C
[11]	N/A	SW-01	Solution-annealed and soaked in test environment for 14 days	≈ 7 dpa	Simulated PWR water environment at 228–318 °C

* Detail of the heat treatment was not provided in the reference.

stress, the modified strip-yield model [24] employed in the present study is applicable for arbitrary two-dimensional cracked geometries and loading types. This model [24] considers the effects of both crack tip plasticity and the plastic wake, and has been successfully used for fatigue crack propagation prediction in an edge-cracked two-dimensional bodies.

In the present work, rigid-perfectly plastic bar elements were used to model the plastic zone at crack tip. The plastic region of length ρ ahead of the actual crack was modeled using ten elements, while an initial crack of length a_i was modeled using five elements. The plastic zone size was determined by incorporating a weight function-based computational and the amount of crack extension, Δa, was defined as [24]:

$$\Delta a = 0.05\rho_{max} \tag{2}$$

where ρ_{max} represents the plastic zone length under the maximum applied load.

Due to the crack closure phenomenon, Elber [26] suggested that only a portion of the loading cycle attributes to the crack propagation in which the crack is fully open. Hence, the effective stress intensity factor range, ΔK_{eff}, is suggested to be used in place of the stress intensity factor range, ΔK, especially at low growth rates approaching the threshold. The effective stress intensity factor range can be defined as [24]:

$$\Delta K_{eff} = K_{max} - K_0 = K[S_{max}h(x)] - K[S_0h(x)] \tag{3}$$

where $S_{max}h(x)$ is the maximum applied stress with a scaling parameter S_{max}, $S_0h(x)$ is the crack opening stress with a scaling parameter S_0, and $h(x)$ functional crack relationship of the crack opening stress along the line of crack propagation (i.e., weight function).

The fatigue crack growth rate can be represented as a power function of ΔK_{eff}, known as the modified Paris-Elber equation [26]:

$$\left(\frac{da}{dN}\right)_{fatigue} = C(\Delta K_{eff})^m \tag{4}$$

To obtain the parameters C and m in Eq. (4), the following relationships may be employed [25,27]:

$$\left(\frac{da}{dN}\right)_{fatigue} = C_1(\Delta K_{eff})^{C_2}\left[\frac{1-\left(\frac{\Delta K_0}{\Delta K_{eff}}\right)^2}{1-\left(\frac{K[S_{max}h(x)]}{C_5}\right)^2}\right] \tag{5}$$

where

$$\Delta K_0 = C_3\left(1 - C_4\frac{S_0}{S_{max}}\right) \tag{6}$$

In Eqs. (5)-(6), the constants C_1 and C_2 are determined from the constant amplitude rate data, while C_3 and C_4 are obtained from the threshold data, and C_5 is the fracture toughness. Consider Eq. (4) and the Paris equation, the constant C_2 in Eq. (5) is essentially the coefficient m [25], which can be equated to the slope of the fatigue crack growth rate for the Paris Equation. For austenitic stainless steel, m = 3.25 [28], while the coefficients C_3 and C_4 are 2.97 MPa-√m and 0.8, respectively [25,29]. The fracture toughness, K_c, or the coefficient C_5, for SS 304 is 119 MPa-√m.

In the present study, the Forman equation has been suggested to better represent the fatigue crack growth rate for Types 304L, 316, and 316L SS as compared to the other fatigue crack growth models [30]. According to the Forman equation, the crack growth per cycle is given by [31]:

$$\left(\frac{da}{dN}\right)_{fatigue} = \frac{C(\Delta K)^m}{(1-R)K_c - \Delta K} \tag{7}$$

The fracture toughness, K_c, is 112 MPa-√m for SS 316 and SS 316L, and 119 MPa-√m for SS 304L.

The crack opening stress, S_0, the maximum applied stress, S_{max}, and the effective stress intensity factor range, ΔK_{eff}, are first calculated based on the experimental data (i.e., K_{max} and ΔK). The coefficient C_1 in Eq. (6) and the coefficient C in Eq. (7) can be obtained to fit the data based on irradiated specimens under the water environment. The constant values for each selected material are given in Table 5.

3.2. Creep crack growth model

Although various strip-yield models have been primarily proposed to simulate fatigue crack growth under constant and variable amplitude loading, only a few numerical analyses based on the strip-yield methodology have been developed to take into account the presence of local creep strains [32–35]. Creep crack initiation and growth in most materials begins with the initial stage of cracking in which there is a buildup of damage near the crack tip known as the incubation period, as seen in Fig. 1. At time less than the incubation period ($t < t_i$), the blunting of the crack tip between the two crack faces occurs. As time increases to initiation time ($t = t_i$), the displacement increases and reaches a critical crack tip opening displacement, ϕ_c, and the measurable crack extension and growth can be detected. The crack then subsequently advances at time greater than initiation time ($t < t_i$) [36,37].

In the present study, the crack initiation time, t_i, due to creep is predicted based on the critical crack tip opening displacement, ϕ_c. By considering the strip-yield model based on a critical crack tip opening displacement criterion [34], the crack tip opening displacement, ϕ, due to constant load can be related to the creep strain as:

$$\phi = \rho(\varepsilon_o + \varepsilon_s) \tag{8}$$

where the primary and secondary creep strain is represented by ε_o and ε_s, respectively, and ρ is the length of plastic zone ahead of the crack. In the primary creep, Andrade's law can be utilized to describe the hardening state of a material under isothermal creep condition, and the relationship between the maximum applied stress, σ_{max}, plastic creep strain, ε_p, and plastic creep strain rate, $\dot{\varepsilon}_p$ in the plastic zone as [38]:

$$\sigma_{max} = k(\varepsilon_p)^{\frac{1}{M}}(\dot{\varepsilon}_p)^{\frac{1}{J}} \tag{9}$$

where k, M, and J are the coefficient of resistant, viscosity exponent, and hardening exponent, respectively. These parameters are temperature and material-dependent [38]. It should be noted that, to our best

Table 3
Fatigue crack growth specimens and test conditions for Type 316 stainless steels [10,11].

Reference	Test #	Specimen #	Pre-treatment	Radiation	Test Condition
[10]	CGRI-25	C21-A	Heat C21*	3.0×10^{20} n/cm^2 (0.45 dpa) at ≈ 288 °C	High-purity water with ≈ 350 ppb DO at 289 °C
	CGRI-24	C21-B	Heat C21*	9.0×10^{20} n/cm^2 (1.35 dpa) at ≈ 288 °C	High-purity water with ≈ 350 ppb DO at 289 °C
	CGRI-26	C21-C	Heat C21*	2.0×10^{21} n/cm^2 (3.0 dpa) at ≈ 288 °C	Water with ≈ 500 ppb DO at 289 °C
[11]	BR-01	N/A	Cold-worked and soaked in test environment at ≈ 320 °C for ≈ 10 days	≈ 5 dpa	High-purity water with low DO (< 10 ppb)
	CR-01	N/A	Cold-worked and soaked in test environment at ≈ 320 °C for ≈ 10 days	≈ 7 dpa	High-purity water with low DO (< 10 ppb)
	CR-04	N/A	Cold-worked and soaked in test environment at ≈ 320 °C for ≈ 8 days	≈ 8 dpa	Simulated PWR water environment at 228–318 °C

* Detail of the heat treatment was not provided in the reference.

knowledge, these material constants that are entirely suitable for the BWR condition (i.e., 289 °C) are not available in the literature. Therefore, the values of k, M, and J for the selected materials at 20 °C and 550 °C were employed in this study as an initial approximation, as given inTable 5.

For a constant stress with zero initial plastic strain ($\varepsilon_p(0) = 0$), Eq. (9) can be integrated to determine the primary creep strain as:

$$\varepsilon_o = \left[\frac{J+M}{M}\left(\frac{\sigma_{max}}{k}\right)^J\right]^{\frac{M}{J+M}} \Delta t_{hold}{}^{\frac{M}{J+M}} \tag{10}$$

where Δt_{hold} in Eq. (10) represents the hold-time for creep. For secondary creep, the modified Norton's Power Law may be utilized for SS304 and SS304L [39], and SS316 and SS316L [38] to determine the creep strain rate for elements in the plastic zone as:

$$\dot{\varepsilon}_s = A_s(\sigma_{max})^{n'} \; exp\left(-\frac{Q}{R^*T}\right) \quad \text{for Types 304 and 304L SS} \tag{11}$$

$$\dot{\varepsilon}_s = \left(\frac{\sigma_{max}}{\zeta}\right)^{n^*} \quad \text{for Types 316 and 316L SS} \tag{12}$$

where, in Eq. (11), A_s is the secondary creep strain coefficient ($A_s = 0.097838\,\text{MPa}^{-n'}\text{-hr}^{-1}$), n' is the secondary creep exponent for Types 304 and 304L SS ($n' = 4.59$), Q is the activation energy ($Q = 260{,}000$ J/mol), R^* is the Boltzman gas constant ($R^* = 8.31$ J/(mol-K), and T is the absolute temperature ($T = 562.15$ K) [39]. In Eq. (12), ζ is the secondary creep strain coefficient ($\zeta = 765$ MPa-hr) and n^* is the secondary creep exponent for Types 316 and 316L SS ($n^* = 8.2$) [38]. Similar to the previous procedure to determine the primary creep strain, Eqs. (11) and (12) can be integrated to obtain the plastic strain for secondary creep, which can be represented as:

$$\varepsilon_s = \rho A_s(\sigma_{max})^{n'} exp\left(-\frac{Q}{R^*T}\right)\Delta t_{hold} \quad \text{for Types 304 and 304L SS} \tag{13}$$

$$\varepsilon_s = \rho\left(\frac{\sigma_{max}}{\zeta}\right)^{n^*} \Delta t_{hold} \quad \text{for Types 316 and 316L SS} \tag{14}$$

Once the primary and secondary creep strains are obtained, the creep damage in the plastic zone can be determined. This is accomplished by calculating the crack opening displacement, ϕ, due to creep and utilizing its relation to the flow stress (i.e., the compressive stress applied to the elements in the plastic zone), σ_o, for the increment from time l to $l+1$ as [40,35]:

$$\sigma_{oo_{l+1}} = \frac{\sigma_{max} f(x_i) - \phi_{l+1}}{\sum_{j=1}^{n_{el}} g(c,x_j)} \tag{15}$$

where σ_{oo} is the flow stress at the crack tip element, $f(x_i)$ is the displacement of crack for an applied stress, σ_{max}, ϕ_{l+1} is the displacement of the crack tip at $l+1$ iteration, and $g(c,x_j)$ is the displacement for the contact stresses applied in the plastic zone. The $f(x_i)$ and $g(c,x_j)$ are influence functions which are given in [25].

After the initial calculation of the primary creep strain, the displacement in primary creep is adjusted to the following equations for the plane strain and plane stress conditions [34]:

$$\phi_o = \frac{(4(1-\nu)\sigma_{oo}a_i)}{\pi G} ln\left[sec\left(\frac{\pi\sigma_{max}}{2\sigma_{oo}}\right)\right] \quad \text{for plane strain} \tag{16}$$

$$\phi_o = \frac{(8\sigma_{oo}a_i)}{\pi E} ln\left[sec\left(\frac{\pi\sigma_{max}}{2\sigma_{oo}}\right)\right] \quad \text{for plane stress} \tag{17}$$

where υ is the Poisson's ratio, G is the shear modulus, and E is the modulus of elasticity. The creep strain from Eqs. (13) and (14) are combined with the initial crack opening displacement, ϕ_o, to obtain the critical crack tip opening displacement, ϕ_c, which represents the crack

Table 4
Fatigue crack growth specimen and test condition for Type 316L stainless steels [10].

Test #	Specimen #	Pre-treatment	Radiation	Test Condition
CGRI-09	C16-B	Heat C16*	2×10^{21} n/cm^2 (3 dpa) at ≈ 288 °C	High-purity water with ≈ 250 ppb DO at 289 °C

* Detail of the heat treatment was not provided in the reference.

opening displacement at the end of the incubation period (see Fig. 1).

$$\phi_c = \phi_o + \rho A_s (\sigma_{max})^{n'} exp\left(-\frac{Q}{R^* T}\right)\Delta t_{hold} \quad \text{for Types 304 and 304L SS} \tag{18}$$

$$\phi_c = \phi_o + \rho\left(\frac{\sigma_{max}}{\zeta}\right)^{n^*}\Delta t_{hold} \quad \text{for Types 316 and 316L SS} \tag{19}$$

Then, the flow stress at the end of the incubation period, σ_{oi}, can be obtained from the following equations [34]:

Table 5
Parameters used in the study for estimating fatigue crack growth with hold-time and irradiation effects for Types 304, 304L, 316, and 316L stainless steels.

Parameters	Material			
	304 SS	304L SS	316 SS	316L SS
C_1 or C	6.536×10^{-15}	8.293×10^{-13}	4.028×10^{-12}	3.925×10^{-11}
C_2 or m [28]	3.25			
C_3 [25]	2.97 MPa-√m	–	–	–
C_4 [25]	0.8	–	–	–
C_5 or K_c [14]	119 MPa-√m		112 MPa-√m	
k (at 20 °C) [38]	65			
k (at 550 °C) [38]	65		120	
M (at 20 °C) [38]	5		14	
M (at 550 °C) [38]	5		6	
J (at 20 °C) [38]	752 MPa-s		458 MPa-s	
J (at 550 °C) [38]	752 MPa-s		494 MPa-s	
A_s [39]	0.097838 MPa$^{-n'}$-hr^{-1}		–	–
n' [39]	4.59		–	–

Parameters	Material			
	304 SS	304L SS	316 SS	316L SS
Q [39]	260,000 J/mol		–	–
R^* [44]	8.31 J/(mol-K)		–	–
T	562.15 K (Reactor Temperature 289°C)		–	–
ζ [38]	–	–	765 MPa-hr	
n^* [38]	–	–	8.24	
υ [14]	0.305			
G [14]	73.1 GPa			
B [22]	0.33			
$\tilde{r}_c$ [22]	0.387			
A_c [22]	9.53×10^{-21} MPa^{-1}-hr^{-1}			
N' [45]	8		8.2	
ε_f [45]	0.4			

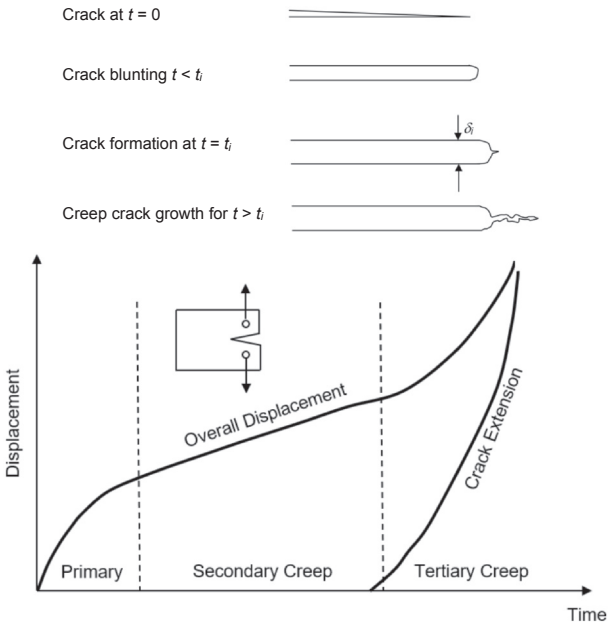

Fig. 1. Schematic behavior of creep crack blunting, initiation, and growth [36,37].

$$\phi_c = \frac{(4(1-\nu)\sigma_{oi}a_i)}{\pi G} ln\left[sec\left(\frac{\pi\sigma_{max}}{2\sigma_{oi}}\right)\right] \quad \text{for plane strain} \tag{20}$$

$$\phi_c = \frac{(8\sigma_{oi}a_i)}{\pi E} ln\left[sec\left(\frac{\pi\sigma_{max}}{2\sigma_{oi}}\right)\right] \quad \text{for plane stress} \tag{21}$$

In Eqs. (20) and (21), for a given hold-time, the flow stress at the crack tip initiation, σ_{oi}, is obtained from the critical crack tip opening displacement for a given hold-time. The following equations were employed simultaneously with Eqs. (20) and (21) to calculate the crack initiation time, t_i, [34]:

$$\frac{t_i}{\Delta t_{hold}} = \frac{(B_n(\alpha_i) - B_n(\alpha_o))}{B(\alpha_i)} \tag{22}$$

where

$$B_n(\alpha) = \int_0^{\alpha}\left(\frac{2\theta}{\pi}\right)^n\left(\frac{dB(\theta)}{d\theta}\right)d\theta \tag{23}$$

$$B(\alpha) = \frac{1}{\alpha}\ln(\sec(\alpha)) \tag{24}$$

and

$$\alpha_i = \frac{\pi\sigma_{max}}{2\sigma_{oi}} \tag{25}$$

$$\alpha_o = \frac{\pi\sigma_{max}}{2\sigma_{oo}} \tag{26}$$

Once the initiation time, t_i, is determined, it can be subtracted from the hold-time for creep, Δt_{hold}, to obtain the time when crack growth occurred.

At $t > t_i$, the creep crack extension criterion is employed based on the Nikbin-Smith-Webster (NSW) model that describes the correlation between the creep crack extension rate to the C^* contour integral [41]. For the small-scale creep conditions, the averaged small scale creep parameter over the hold-time, $(C_t)_{avg}$, has been proposed to better characterize the creep-fatigue growth rate in addition to the C^* contour integral, whose analytical expression is given in [42]. The averaged creep parameter is defined as [42]:

$$(C_t)_{avg} = \left[\frac{2\alpha\beta r_c}{Ew}(1-\nu^2)K^4\left(\frac{F'}{F}\right)(EA_c)^{\frac{2}{n^*-1}}\left(N^{\frac{2}{n^*-1}} - (N-1)^{\frac{2}{n^*-1}}\right)\Delta t_{hold}^{\frac{-(n'-3)}{n^*-1}}\right] + C^* \tag{27}$$

where [22]

$$\frac{F'}{F} = \left[\frac{1}{2+\frac{a}{W}} + \left(\frac{3}{2\left(1-\frac{a}{W}\right)}\right)\right] + \left[\frac{4.64 - 26.64\left(\frac{a}{W}\right) + 44.16\left(\frac{a}{W}\right)^2 - 22.4\left(\frac{a}{W}\right)^3}{0.886 + 4.64\left(\frac{a}{W}\right) - 13.32\left(\frac{a}{W}\right)^2 + 14.72\left(\frac{a}{W}\right)^3 - 5.6\left(\frac{a}{W}\right)^4}\right] \tag{28}$$

and [42]

$$\alpha = \frac{1}{2\pi}\left[\frac{(n^*+1)I_{N'}}{2\pi(1-\nu^2)}\right]^{\frac{2}{n^*-1}} \tag{29}$$

In Eqs. (29)-(31), β is the Irwin's correction factor ($\beta = 0.33$), N is the cycle number, $\tilde{\gamma}_c$ is 0.387, n^* is 8.24, and A_c is 9.53×10^{-21} MPa^{-1} hr^{-1} [42,22]. The non-dimensional function $I_{N'}$ in Eq. (29) can be defined as [40]:

$$I_{N'} = 10.3\sqrt{0.13 + \frac{1}{N'}} - \frac{4.6}{N'} \quad \text{for plane strain} \tag{30}$$

$$I_{N'} = 7.2\sqrt{0.12 + \frac{1}{N'}} - \frac{2.9}{N'} \quad \text{for plane stress} \tag{31}$$

where N' is the plastic strain hardening exponent. By defining the averaged creep parameter, $(C_t)_{avg}$, to take the small creep contribution into account, the NSW can be represented as follows:

$$\left(\frac{da}{dt}\right)_{creep} = \frac{(n^*+1)A_c}{\varepsilon_f}\left(\frac{(C_t)_{avg}}{I_{N'}GA_c}\right)^{\frac{n^*}{n^*+1}} r_c^{\frac{1}{n^*+1}} \tag{32}$$

where ε_f is the creep ductility and r_c is the radius of the creep process zone, which is assumed to be equal to the plastic zone length, ρ [40].

3.3. Irradiation correction

The simple monotonic tensile properties of a material are utilized to obtain the radiation correction for a crack growth rate of stainless steel. In this study, the following radiation correction for ultimate tensile strength, σ_u, and yield strength, σ_y, is employed [43]:

$$\sigma_u(dose) \text{ or } \sigma_y(dose) = A_1\left(1 - exp\left(-\frac{dose}{d_o}\right)\right) \tag{33}$$

where $d_o = 3.0$ for water and air and *dose* is the neutron dose imposed on the crack growth.

From the experimental data employed in the present study, the fracture toughness of Types 304, 304L, 316, and 316L SS is found to decrease as dose increases [10,11]. It was also observed that, as the radiation dose of 0.75–4 dpa, the crack growth rates increases by 2–7 times as compared to those of un-irradiated specimens [10]. On the other hand, at the neutron dose of 0.45 dpa or less, insignificant neutron dose on the crack growth rate of stainless steels in BWR environment is noted [10]. Moreover, the minimum effect of irradiation on crack growth in air is also observed for stainless steels irradiated up to 2.2 dpa. As a result, A_1 in Eq. (36) equal to $\left(\frac{5}{3.25}\right)(dose)\frac{da}{dN}$ is adopted, where $\frac{da}{dN}$ is the crack growth rate for one cycle. The final form of the crack growth due to fatigue for irradiated specimen is as follows:

$$\left(\frac{da}{dN}\right)_{irrad} = \left(\frac{5}{3.25}\right)(dose)\left(\frac{da}{dN}\right)_{fatigue}\left(1 - exp\left(-\frac{dose}{3}\right)\right) \quad (34)$$

4. Crack growth predictions and discussions

4.1. Irradiated specimens subjected to cyclic loading without hold-time

Using the methodology presented in this study, the crack length for given cycles for irradiated specimens subjected to cyclic loading without hold-time are estimated. These are Type 304L SS C3-A, Type 304L SS C3-B, Type 304L SS C3-C, and Type 316L SS C-16B specimens. The pre-heat treatment and test environment for these specimens are provided in Tables 3 and 4 for Type 304L SS and Type 316L SS, respectively. The observed and estimated crack length versus cycles are displayed in Fig. 2(a) – (d) for specimens C3-A, C3-B, C3-C, and C-16B, respectively.

For specimen C3-A, a satisfactory correlation between the experimental and estimated crack growth is obtained, with all estimated crack length are within a factor of 3 scatter bands, as displayed in Fig. 3(a). As reported in [10], the fatigue behavior of a specimen irradiated to neutron fluence of less than 0.45 was observed to be similar to that of un-irradiated specimen. Hence, the model presented in this study was built around the premise that 0.45 dpa would minimally affect the crack growth. Moreover, since specimen C3-A was irradiated to a low dose contribution of 0.45 dpa and no dwell creep, the fatigue portion of the model is regarded to be the main contributor to this specimen's crack growth. The fatigue portion of the model was able to reasonably predict the crack opening stress. In this case, the opening stress appears to be stable as the plastic zone expands and the crack length propagates.

The comparison of the experimental and predictive crack length for specimens C3-B and C3-C, along with scattering bands of 3 and 5 are displayed in Fig. 3(b) and 3(c), respectively. Poor correlations are observed for both specimens with less than 30% of the estimated data within the scatter bands of 5. The model appears to suffer from the fatigue contribution in which the opening stress equation was not able to predict enough crack growth. The force contribution to the fatigue due to the maximum stress, S_{max}, was not enough to overcome the forces in the plastic zone to increase the crack growth. The corrosion fatigue and the stress corrosion cracking may possibly be a contributor along with the irradiation in the C3-B and C3-C specimens. There was no creep which leads to the conclusion that the radiation model for SS 304L may warrant investigating to emphasize the contribution to fatigue loading. In addition, a poor approximation could be due to the limited data points beyond pre-cracking. The given data points may not be enough to develop the trend in the analysis. Besides, there is no hold-time (as seen in Tables A.3 and A.4), and therefore creep contribution was not included in the analysis. However, the loading rise times in these tests are rather significant especially near the end of the test. Since the rise time effects are not included in the analysis of these specimens, this may further contribute to the poor correlation.

On the other hand, all estimated crack length of Type 316L SS specimen C-16B are within a factor of 3% scatter bands of the experimental data, as displayed in Fig. 3(d). The model seems to work well for determining fatigue and crack contribution due to irradiation. The contribution due to radiation for this particular specimen was 3 dpa, which is in the range of the assumptions used to build the radiation model.

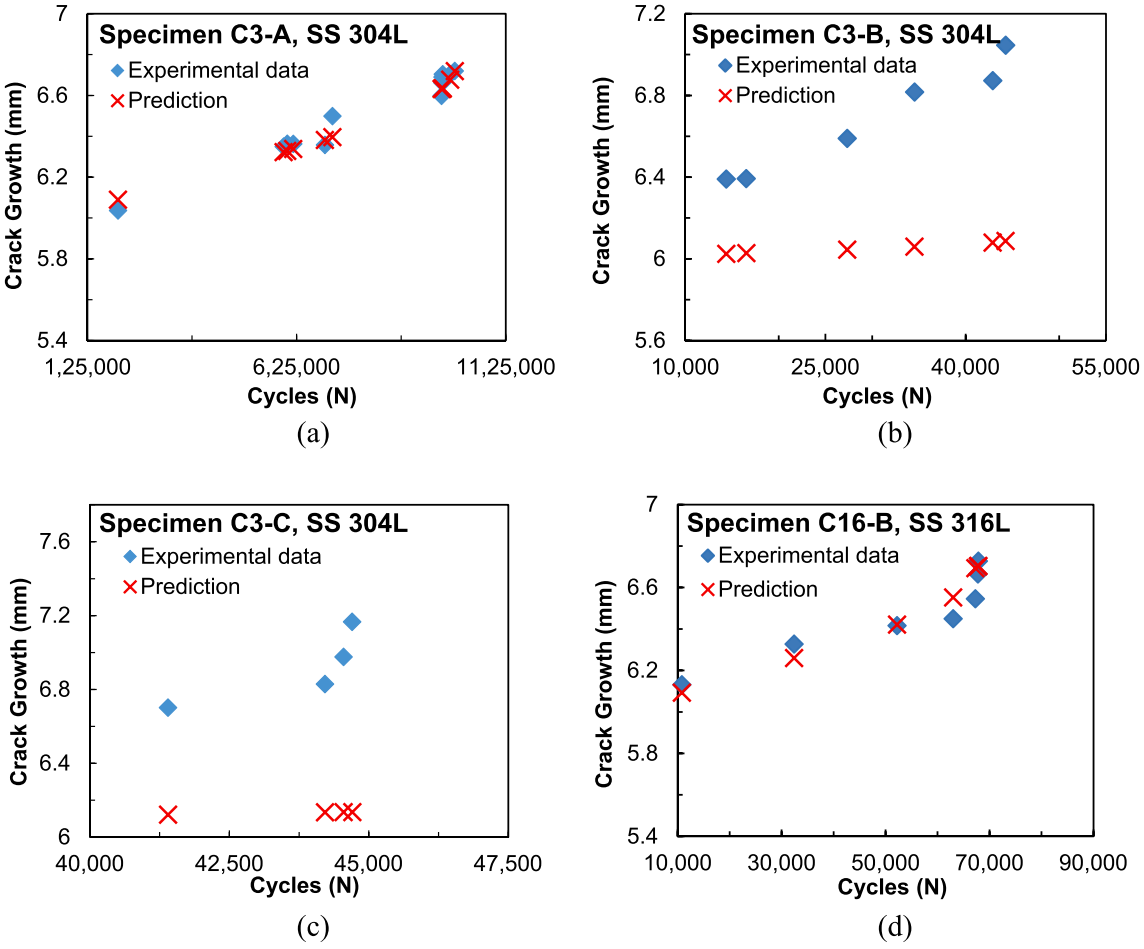

Fig. 2. Crack growth history for given cycles of irradiated specimens subjected to cyclic loading without hold-time.

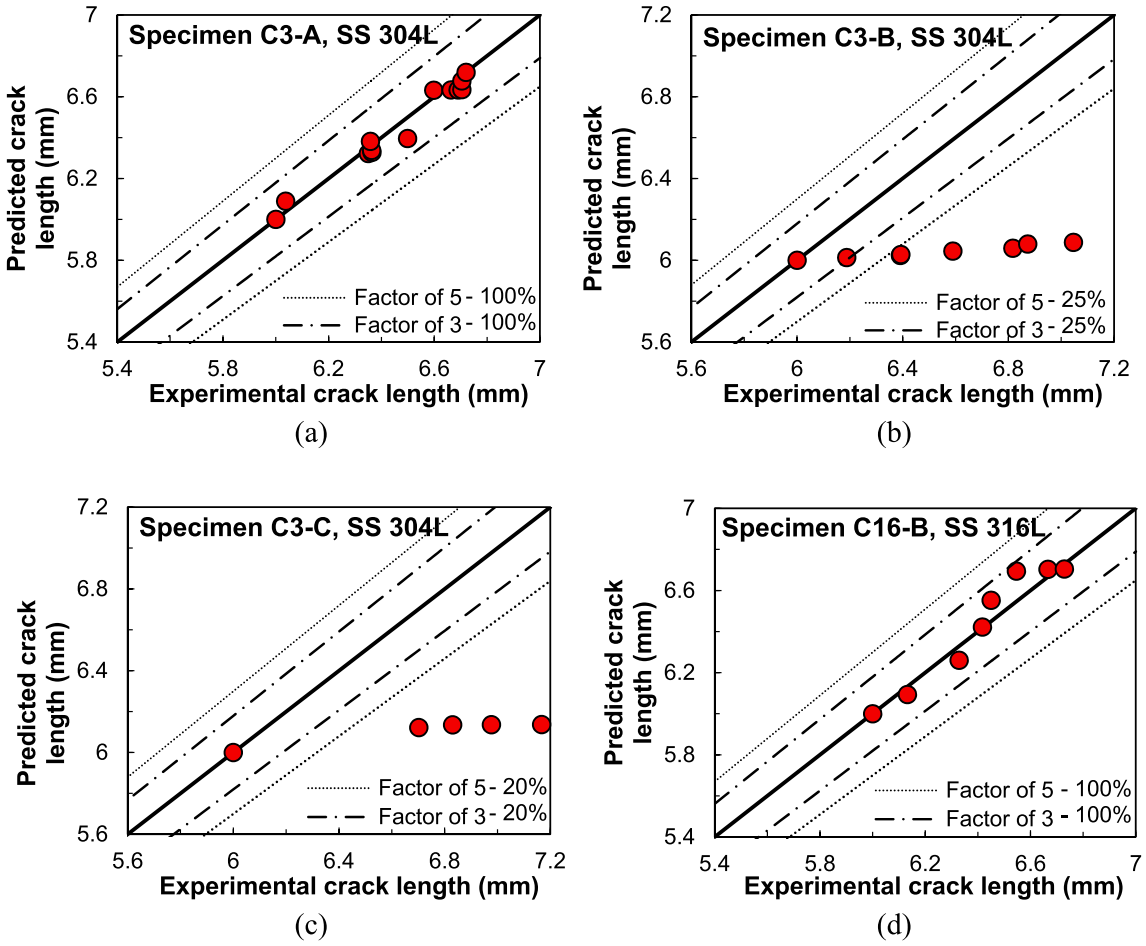

Fig. 3. Predicted crack length of irradiated specimens subjected to cyclic loading without hold-time versus observed crack length with factors of 3 and 5 scatter bands.

4.2. Irradiated specimens subjected to cyclic loading with hold-time

The crack growth at selected cycles for eight irradiated specimens (one Type 304 SS, one Type 304L SS, and six Type 316 SS), which were tested under fatigue loading with hold-times, are estimated. These are specimens 85-3TT (Table 1) and SW-01 (Table 2) presented in Fig. 4, with the plots of the experimental versus estimated crack length of these specimens, superimposed with the scatter bands of 3 and 5, shown in Fig. 5. The estimation results for six Type 316 SS specimens, including specimens C21-A, C21-B, C21-C (Table 3), and specimens from tests BR-01, CR-01, and CR-04 (Table 3), are displayed in Figs. 6 and 7.

The estimated data of specimen 85-3TT in Fig. 4(a) under-predicted the crack growth rate. As the crack growth progressed, the ΔK decreased, causing the minimum stress to increase and the stability of the opening stress to be challenged. Approximately 80% and 100% of the estimated crack length of specimen 85-3TT are within the scatter bands of 3 and 5, respectively, as seen in Fig. 5(a). On the other hand, the

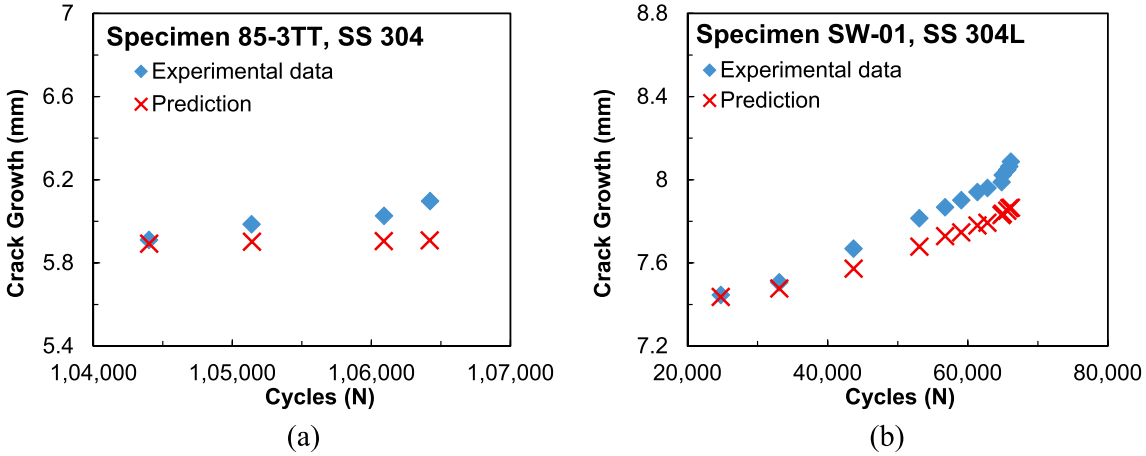

Fig. 4. Crack length history of irradiated SS 304 and SS 304L specimens subjected to cyclic loading with hold-time.

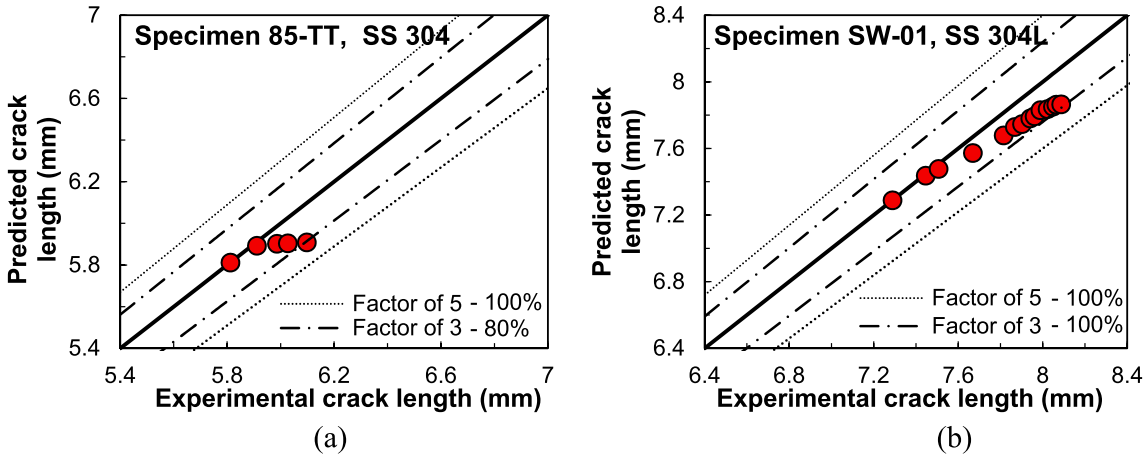

Fig. 5. Predicted crack length of irradiated SS 304 and SS 304L specimens subjected to cyclic loading with hold-time versus observed crack length with factors of 3 and 5 scatter bands.

fatigue-creep, and radiation contribution of the model seems to work reasonably well for specimen SW-01 as seen in Fig. 4(b). The model demonstrated a positive trend with the applied stress intensity factors. There appears no corrosion fatigue or stress corrosion cracking environment enhancement. The contact stress calculation from the minimum stress that was later used as an input to obtain the opening stress was found to be stable. As illustrated in Fig. 5(b), all estimated crack length data of specimen SW-01 are within a factor of 5 scatter bands.

Reasonable crack growth estimations are obtained for specimens SS 316 C21-A, C21-B, and C21-C, as displayed in Fig. 6(a) −6(c), respectively. Specimen C21-A was subjected to a low dose of 0.45 dpa. Again, as stated in [10], the specimen with dose equal to or less than 0.45 could be treated as un-irradiated specimen. The model for specimen C21-A accounts for the crack growth with high-stress and low load ratio to some degree. Once the dwell creep initiates on the three two data points, the model appears to work well. In addition, two sets of specimen C21-B data were lost at time equal 24 h and 30 h. The remaining 5000 cycles illustrated in Fig. 6(b) is essentially over 150 h period. For specimen C21-C in Fig. 6(c) that was irradiated to 3 dpa, the radiation contribution of the model can be seen in the two end points. Similar to specimens C21-A and C21-B, the model for specimen C21-C accounts for the opening stress contribution to crack growth. Approximately 75% of the estimated data are within 3% scatter bands as displayed in Fig. 7(c).

As shown in Fig. 6(d)-6(f), acceptable crack growth estimations are obtained for the three Type 316 SS specimens, which were irradiated to high neutron fluences of 5–8 dpa, and tested in the PWR water environment. Moreover, at the beginning of the test BR-01 (Fig. 6(d)), the estimated crack growth is significantly larger as compared to the experimental data. For these initial cycles, the fatigue-creep contribution of the model demonstrates small crack growth along with the data, while the irradiation contribution estimates significant crack growth up to approximately 290,000 cycles where the stress intensity factor changes. The high applied stress and low load ratio test condition during these cycles may lead to the instability of the model, and inability to solve the opening stress. At around 350,000 cycles, the experimental data shows a significant increase in the crack growth due to environmental enhancement, and the model enhances the effect of radiation as the crack growth progresses. Approximately 90% of the estimated data for the specimen in Test BR-01 is within 5% scatter bands, as displayed in Fig. 7(d).

In Fig. 6(e), the stable crack growth of the Type 316 SS specimen in test CR-01 was quickly established. However, the test was restarted around 55,000 cycle due to a leak during testing which caused the autoclave heater to trip. The stable crack growth from environment enhancement was lost and had to be re-established. The model then slightly over-estimated the stable crack growth, which may due to the temperature perturbation when the heater was restarted. Since the model is based on the isothermal condition, the changes in temperature may contribute to the anomalies in the model estimation. Nonetheless, as illustrated in Fig. 7(e), the model was able to estimate the crack growth reasonably well. On the other hand, Type 316 SS specimen in Test CR-04 was subjected to a low maximum stress intensity factor that was initially applied, as well as a large dose of 8 dpa which is considered to be a significant contributor to the crack growth. These may contribute to the poor correlation (i.e., 28% within 5% scatter bands) between the experimental and estimated crack length was obtained for, as shown in Fig. 7(f). In addition, the poor correlation could be from the environmental effects from the oxygen addition. This specimen was tested in a typical PWR condition and more information regarding the test environment is needed.

5. Conclusions

The crack growth approximation model for irradiated austenitic SS was presented in this study. The model was derived for several austenitic SS, including Types 304, 304L, 316 and 316L SS, which are typically used to construct core internal components of nuclear reactors. Using the superposition technique, existing fatigue and creep crack growth models based on the modified strip-yield methodology were employed and extended to include the effects of irradiation. Based on the analyses presented in this study, the following conclusions can be drawn:

(1) By utilizing the crack length data for irritated materials subjected to either cyclic loading without hold-time or cyclic loading with hold-time (i.e., combined fatigue-creep), one was able to obtain the irradiation contribution of the crack growth approximation model to determine the crack length of irradiated SS at given cycles. Although acceptable correlations between the observed and approximated crack growth were obtained for both un-irradiated and irradiated SS specimens subjected to various test conditions, more experimental data is still needed to better support the results.
(2) By employing the modified Paris-Elber equation in the fatigue crack growth model for Type 304L SS materials, poor correlation was observed for specimens that are exposed to dissolved oxygen environment. Additional analysis should, therefore, be performed to obtain the effect of oxygen environment on fatigue crack growth of Type 304L SS.
(3) Modifying the C* contour integral model significantly improved the accuracy of the creep crack growth rate estimations. This was

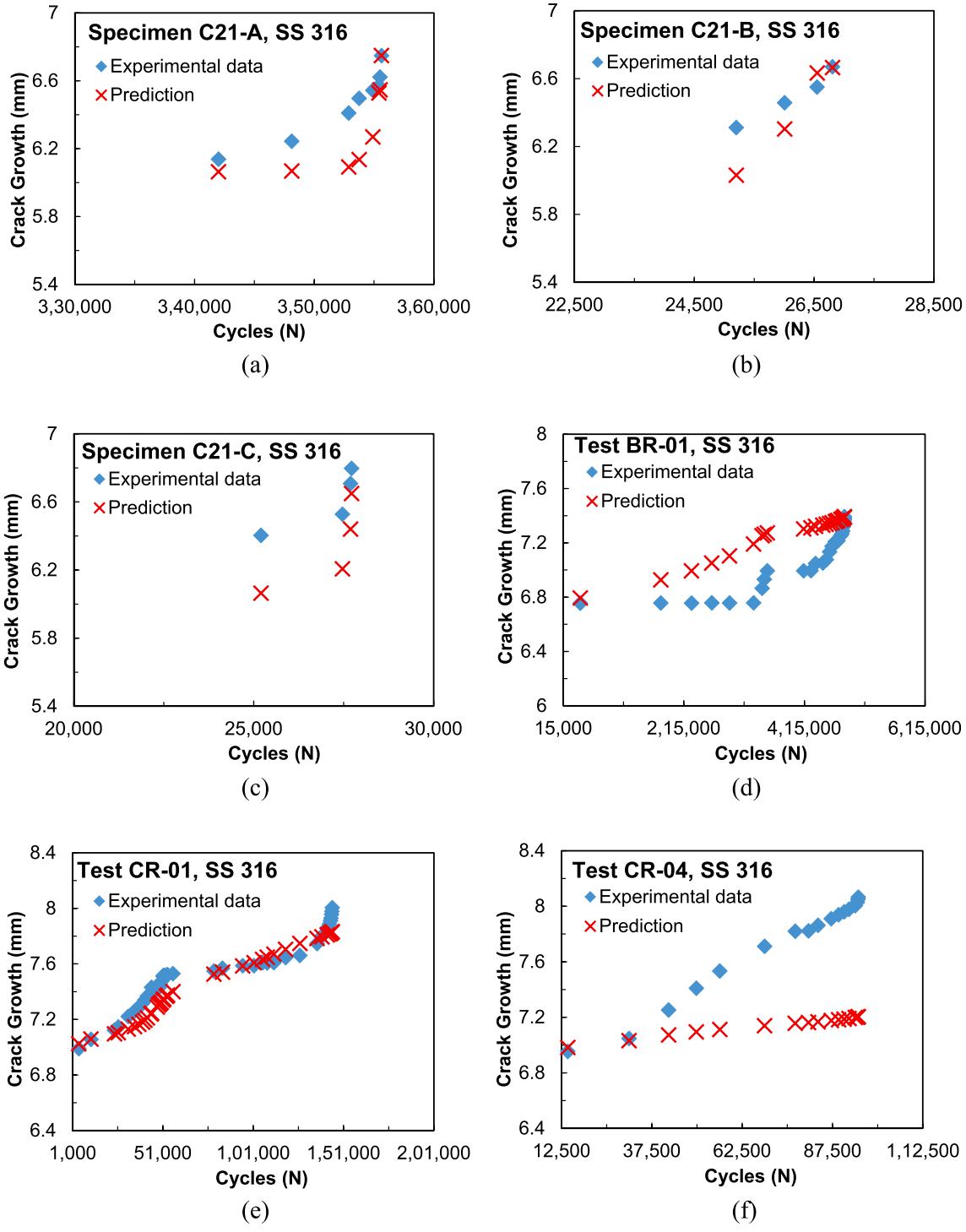

Fig. 6. Crack length history of irradiated SS 316 and SS 316L specimens subjected to cyclic loading with hold-time.

especially noted in irradiated Types 304 (specimen 85-3TT) and 316 SS (specimen CR-01) specimens in water environment, where all the observed and estimated crack length are within the scatter bands of 5.

(4) Creep contribution is included in the proposed model only when the hold-time is present. This also takes the loading rate, as well as position and length of hold-time into account. However, some specimens were subjected to unbalanced cyclic loadings (i.e., slow-fast and fast-slow cycles) with no hold-time, which could potentially lead to some creep damage accumulation that is not accounted for in the analysis, and further investigation is recommended.

(5) The main advantage of the proposed model is the use of superposition to allow the addition of the individual contribution of the physical phenomena into the crack growth material. On the other hands, one of the drawbacks using this model is that different types of materials (i.e., SS 304, SS 316, etc.,) would require individual investigation into the crack growth contributions due to different material makeup, and may require individual set of constants for modeling.

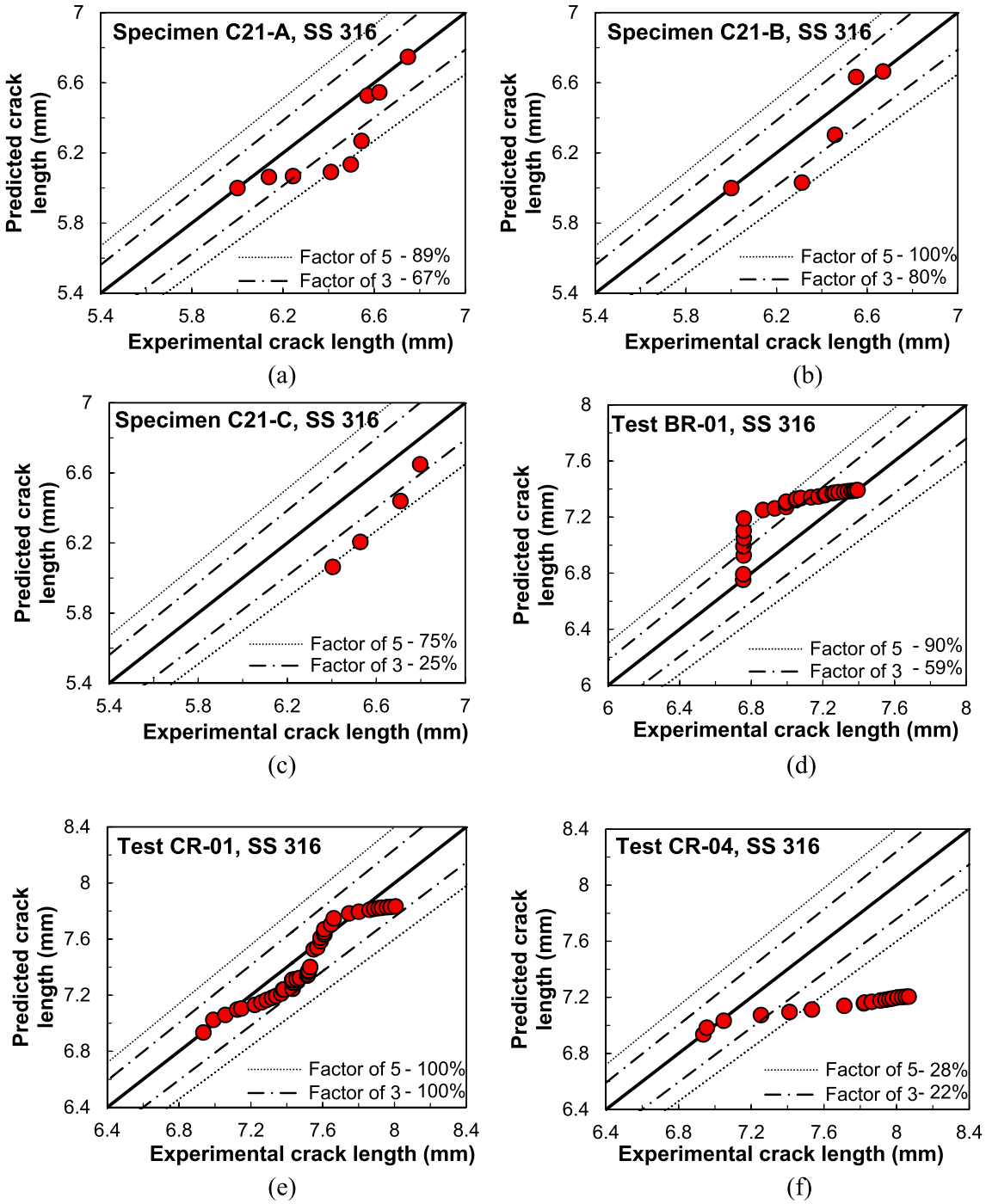

Fig. 7. Predicted crack length of irradiated SS 316 and SS 316L specimens subjected to cyclic loading with hold-time versus observed crack length with factors of 3 and 5 scatter bands.

6. Recommendations

The proposed methodology could be adapted for other materials. In doing so, the irradiation effects on the mechanical properties on the selected material have to be assessed to evaluate the best procedure for developing a radiation model. If a creep model exists for a given material, creep constants have to be determined and assessed. In addition, since the proposed methodology is intended for first-hand fatigue and creep calculations, considerable additional analysis as well as experimental data for validation are required for a better understanding of the material degradation process to obtain more accurate crack growth predictions for components and structures in the reactor environment. Such information is considered crucial for safe and reliable reactor operations as well as their life extensions. For future studies, the effects of stress corrosion cracking (SCC) should be investigated using the principle of superposition to obtain the SCC contribution in conjunction with radiation, which will greatly improve the accuracy of the model to estimate the crack growth for irradiated materials in the light water reactors environment.

CRediT authorship contribution statement

Robert W. Fuller: Conceptualization, Methodology, Software, Writing - original draft. **Jutima Simsiriwong:** Conceptualization,

Writing - original draft, Writing - review & editing, Visualization. **Nima Shamsaei:** Conceptualization, Writing - review & editing, Supervision.

Declaration of Competing Interest

We wish to confirm that there are no known conflicts of interest associated with this publication and there has been no significant financial support for this work that could have influenced its outcome.

Appendix A. Supplementary material

Supplementary data to this article can be found online at https://doi.org/10.1016/j.tafmec.2020.102759.

References

[1] B.K. Grimes, US Nuclear Regulatory Commission Washington DC, Information Notice No. 93-101: Jet Pump Hold-Down Beam Failure, December 1993.
[2] K. Kussmaul, D. Blind, J. Jansky, R. Rintamaa, Formation and growth of cracking in feed water pipes and RPV nozzles, Nucl. Eng. Des. 81 (1) (1984) 105–119.
[3] K. Lida, A review of fatigue failures in LWR plants in Japan, Nucl. Eng. Des. 138 (3) (1992) 297–312.
[4] O.K. Chopra, Mechanism and estimation of fatigue crack initiation in austenitic stainless steels in LWR environments NUREG/CR-6787 ANL-01/25, Nucl. Regulat. Commission (2001).
[5] American Society of Mechanical Engineers (ASME). Rules for Construction of Nuclear Power Plant Components. ASME Boiler and Pressure Vessel Code, Section III, Division 1 - Subsection NE, Class MC Components, ASME, New York, New York, 1992.
[6] A.F. Rowcliffe, M.L. Grossbeck, The response of austenitic steels to radiation damage, J. Nucl. Mater. 122 (1) (1984) 181–190.
[7] D.J. Michel, H.H. Smith, Deformation microstructure developed during fatigue crack propagation in type 316 stainless steel at 593°C, in: Effects of Radiation on Materials. ASTM STP 782. ASTM International 1982, pp. 690–700.
[8] W.J. Shack, T.F. Kassner, Review of environmental effects of fatigue crack growth of austenitic stainless steels NUREG/CR-6176 ANL-94/1, Nucl. Regulat. Commission (1994).
[9] L.A. James, The effect of fast neutron irradiation upon the fatigue-crack propagation behavior of two austenitic stainless steels, J. Nucl. Mater. 59 (2) (1976) 183–191.
[10] O.K. Chopra, W.J. Shack, Crack growth rates and fracture toughness of irradiated austenitic stainless steels in BWR environments NUREG/CR-6960 ANL-06/58, Nucl. Regulat. Commission (2008).
[11] Y. Chen, B. Alexandreanu, K. Natesan, Technical letter report on the cracking of irradiated stainless steels in low-corrosion-potential environments ANL-13/12, Nucl. Regulat. Commission (2013).
[12] W.S. Hazelton, W.H. Koo, Technical report on material selection and processing guidelines for BWR coolant pressure boundary piping NUREG-0313 Rev. 2, Nucl. Regul. Commission (1998).
[13] M. Bakirov, Impact of operational loads and creep, fatigue and corrosion interactions on nuclear power plant systems, structures and components (SSC), in: Understanding and Mitigating Ageing in Nuclear Power Plants, Woodhead Publishing, 2010.
[14] Eugene A. Avallone, Marks' standard handbook for mechanical engineers, The McGraw-Hill Companies Inc, 2007.
[15] E. Krempl, An experimental study of room-temperature rate-sensitivity, creep and relaxation of AISI type 304 stainless steel, J. Mech. Phys. Solids 27 (5–6) (1979) 363–375.
[16] C. Liu, P. Liu, Z. Zhao, D.O. Northwood, Room temperature creep of a high strength steel, Mater. Des. 22 (4) (2001) 325–328.
[17] M.E. Kassner, P. Geantil, R.S. Rosen, Ambient temperature creep of type 304 stainless steel, J. Eng. Mater. Technol. 133 (2) (2011).
[18] M.E. Kassner, K. Smith, Low temperature creep plasticity, J. Mater. Res. Technol. 3 (3) (2014) 280–288.
[19] K.H. Luk, Boiling-Water Reactor internals aging degradation study. Phase 1. NUREG/CR-5754; ORNL/TM-11876. Nuclear Regulatory Commission, 1993.
[20] Y.S. Garud, Low temperature creep and irradiation creep in nuclear reactor applications: A critical review, Int. J. Press. Vessels Pip. 139 (2016) 137–145.
[21] G.S. Was, Fundamentals of Radiation Materials Science: Metals and Alloys, Springer, 2016.
[22] S.B. Narasimhachary, A. Saxena, Crack growth behavior of 9Cr− 1Mo (P91) steel under creep–fatigue conditions, Int. J. Fatigue 56 (2013) 106–113.
[23] ASTM E2760-16, Standard Test Method for Creep-Fatigue Crack Growth Testing, ASTM International, West Conshohocken, PA, 2016.
[24] S.R. Daniewicz, J.A. Collins, D.R. Houser, An elastic-plastic analytical model for predicting fatigue crack growth in arbitrary edge-cracked two-dimensional geometries with residual stress, Int. J. Fatigue 16 (2) (1994) 123–133.
[25] J.C. Newman, A crack-closure model for predicting fatigue crack growth under aircraft spectrum loading, in: Methods and models for predicting fatigue crack growth under random loading, ASTM STP 748, ASTM International, 1981, pp. 53–84.
[26] W. Elber, Fatigue crack closure under cyclic tension, Eng. Fract. Mech. 2 (1) (1970) 37–44.
[27] J.C. Newman, A crack opening stress equation for fatigue crack growth, Int. J. Fract. 24 (4) (1984) 131–135.
[28] J.M. Barsom, Fatigue-crack propagation in steels of various yield strengths, J. Eng. Ind. 93 (4) (1971) 1190–1196.
[29] M. Lugo, J.B. Jordon, J.D. Bernard, M.F. Horstemeyer, Microstructure-sensitive fatigue modeling of an extruded AM 30 magnesium alloy, SAE Technical Paper No. 2013-01-0980, 2013.
[30] D.W. Hoeppner, W.E. Krupp, Prediction of component life by application of fatigue crack growth knowledge, Eng. Fract. Mech. 6 (1) (1974) 47–70.
[31] R.G. Forman, V.E. Kearney, R.M. Engle, Numerical analysis of crack propagation in cyclic loaded structures, J. Basic Eng. 89 (1967) 459–464.
[32] V. Vitek, A theory of the initiation of creep crack growth, Int. J. Fract. 13 (1) (1977) 39–50.
[33] B.A. Bilby, A.H. Cottrell, K.H. Swinden, The spread of plastic yield from a notch, Proc. Roy. Soc. London A: Math., Phys. Eng. Sci. 272 (1350) (1963) 304–314.
[34] D.J. Ewing, Strip yield models of creep crack incubation and growth, Int. J. Fract. 14 (1) (1978) 101–117.
[35] G. Potirniche, A numerical strip-yield model for the creep crack incubation in steels, ASTM Int. Fatigue Fract. Mech. 9 (3) (2012) 1–13.
[36] J.R. Haigh, The mechanisms of macroscopic high temperature crack growth part I: Experiments on tempered Cr-Mo-V steels, Mater. Sci. Eng. 20 (1975) 213–223.
[37] G.A. Webster, R.A. Ainsworth, High Temperature Component Life Assessment, Chapman & Hall, 1994.
[38] J. Lemaitre, Chaboche, Mechanics of Solid Materials, Cambridge University Press, 1994.
[39] A.H. Sorkhabi, F.V. Tahami, Creep Constitutive Equation for 2-Materials of Weldment-304L Stainless Steel, Int. J. Mech., Aerospace, Ind., Mech. Manuf. Eng. 61 (2012) 710–714.
[40] B.J. Andrews, G. Potirniche, Constituitive creep-fatigue crack growth methodology in two steels using a strip-yield model, Eng. Fract. Mech. 140 (2015) 72–91.
[41] K.M. Nikbin, D.J. Smith, G.A. Webster, An engineering approach to the prediction of creep crack growth, J. Eng. Mater. Technol. 108 (1986) 187.
[42] N. Adefris, A. Saxena, D.L. McDowell, Creep-fatigue crack growth behavior in 1Cr-1Mo-0.25 V steels. Part I: Estimation of crack tip parameters, Fatigue Fract. Eng. Mater. Struct. 19 (4) (1996) 387–398.
[43] R.W. Fuller, N. Shamsaei, J. Simsiriwong, Fatigue life predictions for irradiated stainless steels considering void swellings effects, Eng. Fail. Anal. 59 (2016) 79–98.
[44] L.H. Van Vlack, Elements of Materials Science and Engineering, Reading, MA Addison-Wesley, 1975.
[45] K.M. Nikbin, D.J. Smith, G.A. Webster, Prediction of creep crack growth from uniaxial creep data, Proc. Roy. Soc. London. A. Math. Phys. Sci. 1810 (396) (1984) 183–197.